11th Australasian Fluid Mechanics Conference
University of Tasmania, Hobart, Australia
14-18 December 1992

THERMALS, PUFFS AND MASS SOURCES II - NUMERICAL STUDIES

K.C. NGUYEN, B.R. MORTON and R.W. CRESSWELL

Centre for Dynamical Meteorology
Department of Mathematics, Monash University
Clayton, VIC 3168, AUSTRALIA

ABSTRACT

Large Eddy Simulation (LES) has been used to numerically model two dimensional (line) thermals and puffs. It has been found that the constants in the similarity relations agree with experiments within the applicability of the similarity laws. Variability in the spreading rate and velocity between thermals with the same total buoyancy but differing initial radii and temperatures was also observed. Three dimensional behaviour is an inherent feature of the thermals and is attributed to a hydrostatic instability which is not present in the line puff.

NOTATION

A_o : Area defined by the thermal fluid.
I : Initial momentum per unit length for puff
$2r$: Largest half width.
t : Elapsed time from a fixed virtual time.
z : Height of the thermal front to a fixed virtual origin.
ρ : Density of of the thermal fluid.
ρ_o : Density of of the ambient fluid.
$\Delta\rho$: $\rho_o - \rho$
θ : Local x-averaged temperature.
θ_o : Reference temperature.
$\Delta\theta$: $\theta - \theta_o$

$$\bar{y} = \frac{\int\int y\Delta\theta dydz}{\int\int \Delta\theta dydz} \quad \bar{z} = \frac{\int\int z\Delta\theta dydz}{\int\int \Delta\theta dydz} \quad \sigma_y^2 = \frac{\int\int (y-\bar{y})^2\Delta\theta dydz}{\int\int \Delta\theta dydz},$$

INTRODUCTION

Thermals are compact flows generated by release from rest of a mass of fluid either lighter or heavier than its immediate environment. The range may be extended by including source momentum as well as buoyancy to give forced thermals and, in the extreme case, puffs generated from sources of momentum only.

All turbulent compact flows whether buoyant or not entrain or mix in environmental fluid as they move vertically, and therefore increase in length scale with time. Assumptions of self-similarity may be applied allowing the flow to be described by one length scale and one velocity scale and leading to general laws of flow development based on dimensional and geometrical arguments.

We have seen a sequence of dimensional and laboratory studies on the motion of thermals and puffs in uniform and stratified fluids with the following principal results due to Richards (1963): the motion of a two-dimensional (line) thermal satisfies the similarity laws,

$$z = nr, \qquad z^{3/2} = C(\Delta\rho g A_o/\rho_o)^{1/2}t, \tag{1}$$

and the two-dimensional (line) puff satisfies

$$z = nr, \qquad z^3 = 3n^2 D(It/\rho). \tag{2}$$

Richards carried out a series of laboratory experiments on 'line' thermals generated in water tanks. He found that n and C were constant during each realization, but differed between experiments. He believed that the variability in n and C was due to experimental technique. Tsang (1971) performed a fresh series of experiments on line thermals using a novel source in which he claimed to control the level of disturbances more effectively, The scatter in his results showed that roughly 30% variation remains in C and 20% in n over realizations, though C and n were again sensibly constant in each realization. He claimed that his results would be reproducible if the initial disturbances had been more strickly controlled.

Richards (1965) conducted a further series of laboratory experiments on both axisymmetric and line puffs in a water tank. He found that the constant n was 3.4 for line puffs. He concluded also that the velocity distribution for a puff was very similar to a thermal, within the accuracy of his measurements.

We will restrict our attention wholly to two-dimensional or 'line' thermals and puffs and describe some results from our numerical study.

NUMERICAL SIMULATION OF LINE THERMALS AND LINE PUFFS

We have simulated numerically the motion of a line thermal and a line puff with particular emphasis on similarity solutions. The model employs a large eddy simulation (LES) technique developed by Wyngaard and Brost (1984) in which the resolvable scales of turbulence are modelled directly, while the smaller scales (subgrid) are related to the mean flow by parameterization using an approach due to Deardorff (1980). A cartesian coordinate system has been used with origin at the lowest left corner of the computational box, x parallel to the axis of the line thermal, y horizontal, and z vertical in the opposite direction to the gravity vector. The computational box had 20x50x60 uniformly spaced grid points, and a 2/1 staggered grid system (Harlow & Welch, 1965; Shih & Tan, 1989). The Piacsek and Williams (1970) approach was used to discretize the momentum equations with the exception that the flux corrected transport (FCT) technique (Zalesak, 1979)

was used to discretize the non-linear terms in the temperature and energy equations in order to avoid non-physical oscillations in the scalar variables. A standard central differencing method was used for first derivatives in space and leapfrog time discretization and a time filter for time stepping.

No-slip boundary conditions were applied in the near-wall region together with a logarithmic law of the wall (Ng & Spalding, 1972; Launder & Spalding, 1974). Pressure was handled using the approach of Gresho & Sani (1987) and Gresho (1991); while the first normal derivatives of other scalar variables were set to zero. At the initial time a 'line thermal', consisting of a cylindrical region of warm fluid, was released instantaneously from rest with its axis at the mid (y) point and the 0.2 (z) point in the computational domain. A uniform temperature, $290K$, was taken for the ambient fluid, assumed to be fresh water, and an initial source temperature distribution imposed which was either gaussian or top hat. The flows generated from the two initial distributions will be termed 'gaussian' or 'top hat' thermals. Puffs were released with an initial gaussian momentum distribution only.

Simulation of line thermals

The initial temperature differences between source and ambient fluid are those used by Tsang (1971) and given in his Table 1.

Figures 1(a) and 1(b) show superimposed plots of cross-sectional outlines of the temperature fields for gaussian and top hat thermals, respectively. In the initial stage, the flow is dominated by convection. During this stage, the thermals accelerate upward, showing low levels of mixing with their environment. Once this transient stage of acceleration has passed, however, the thermals entrain more fluid and appear to enter a self-similar regime.

The most striking feature is that the two source profiles, which have been assumed without distinction for many years, produce surprisingly different thermals. It may be argued that the model has failed to manage the steep temperature gradients of the top hat profile, but in that case we might have expected either that oscillations would show in the temperature field or that there would be heat loss, whereas oscillations do not appear beyond the normal level expected from truncation. For one typical test, the heat lost was 0.2%, the error in divergence of order 10^{-5}, and the fluctuation of total energy about its mean value 1.2%.

Figure 2 shows a series of contour plots of temperature for cross-sections of the gaussian thermal at four successive times. Note that despite the fact that these plots are of temperature averaged along the axis of the thermal, there is a 'resolved higher wavenumber' structure after $t = 32s$ towards the leading edge of the flow. Our model is able to resolve features of observed flows such as this, at least to a significant degree.

Similarity and self-similarity

We have given in equations 1 the similarity solution for a line thermal notionally released at time $t = 0$ from a virtual line source of zero width at $z = 0$. For similar flows we expect n and C to be universal constants, but for self-similar flows they will be constant within one realization but will generally differ between realizations. For this part of the discussion of our numerical simulation all results will be averaged in the x direction along the thermal. Questions of similarity are best discussed in terms of weighted means in the yz section.

To find the virtual origin a straight line was fitted to the plot of $\bar{z}$ against σ_y to intersect the z axis at the virtual origin. A plot of $\sigma_y^{3/2}$ against time was also approximately linear and its extension to intercept the time axis gave the time at which the thermal notionally left the virtual origin. The constant n can now be obtained by plotting the height of the front of the thermal above (or below) the virtual origin against the largest halfwidth of the thermal and fitting a straight line of slope n through the data points, as shown in Figure 3(a) for gaussian thermals and Figure 3(b) for top hat thermals. As in Figure 1, Figure 3(a) shows an early stage of vertical slope with little mixing, in which turbulence is presummably growing. Once the thermals are fully developed, an approximately linear relationship between z and r can be seen. The two dashed lines have slopes of 3 and 4, respectively, and our seven numerical simulations, which are for the seven sources used experimentally by Tsang (1971, Table 1), correspond with values in the range $3.0 < n < 3.6$. Tsang stated that his laboratory values for n were about 3 within experimental error, but from his Figure 10 they appear to range from about 3.1 to 3.7. On the other hand, the variability of n appeared was larger in Richards laboratory experiment. He reported values in the range 1.5 to 3.2. We believe that there is an inherent variability in these flows, although this can easily be confused with experimental or numerical errors. From Figure 3(b), the top hat thermal appears to exhibit two distinct similarity regimes in each of the seven tested thermals. A linear relationship between the height of the thermal front and its largest halfwidth may be identified shortly after release while the thermal is still accelerating. This suggests that top hat thermals diffuse quickly across the steep temperature gradient between the thermal fluid and its surroundings. This relationship lasts for approximately half of the observed lifetime of each thermal, after which it changes with corresponding change in slope as the two new frontal lobes grow to significantly influence the flow field. The early slopes are in the range $3.0 \leq n \leq 3.2$ and later slopes in $3.9 \leq n \leq 4.2$.

Values for the constant C in our numerical simulations were obtained by plotting $z^{3/2}\rho_o^{1/2}/(\Delta\rho g A_o)^{1/2}$ against t. For gaussian thermals $1.6 \leq C \leq 1.9$ throughout, whereas for top hat thermals $1.4 \leq C \leq 1.6$ in the initial similarity regime up to $t = 30s$ and $C = 2.5$ for all cases at larger time. Previous values reported by Richards are $1.05 \leq C \leq 3.33$, and $1.7 \leq C \leq 2.3$ by Tsang. There seems to be little doubt that our numerical simulation is generating results of significance, and our model is accurate enough to be used in further studies.

An important feature of our numerical simulation is that the solution curves in Figure 3(a) automatically show the influence of side or top boundaries by change in slope, and it is clear that all of our runs start to be influenced by walls beyond about $2r = 0.60m$ corresponding with $z = 1.30m$ which is about $\frac{3}{4}$ of the height of the $1.80m$ computational box.

Sensitivity studies

The thermals are not only sensitive to their initial geometries such as top hat or gaussian temperature profiles but also depend greatly on other conditions as well. The level of turbulent mixing is one of these. Figures 4(a) and 4(b) are superimposed plots of cross-sectional outlines of the temperature fields for the gaussian thermal with two different turbulent mixing coefficients. The former are ten times smaller and the latter are 5 times larger than the standard value which was used in the calculations presented in the previous discussion. We see that the lower turbulent mixing coefficient corresponds to less entrainment and conversely the higher coefficient leads to larger environmental mixing. Resolvable eddies were observed in the former case but were totally smoothed out in the latter case. Buoyancy is another factor controlling the growth of the thermals. The thermals which have

different initial diameters but have the same amount of initial buoyancy (integrated density deficiency) showed that a larger thermal entrains less but moves upwards more slowly than a smaller thermal, yielding smaller n overall. Also, if two thermals of the same initial size have different amounts of buoyancy, then the most buoyant thermal will spread the least.

Instability

Line thermals were observed to be very unstable in their two-dimensional structures. Small random disturbances were imposed at the instant of release (in order to 'trip' the turbulence) and line thermals were observed to break up and form three-dimensional cells along their axes. This instability was first seen at the leading edge of the thermal where turbulent mixing is strongest. The initial number of cells along the axis of a line thermal appeared to be related to its length and its initial cross-sectional diameter (Figure 5). Unlike laboratory experiments, which showed that the thermal broke up almost immediately after release, the numerical model could only detect these cells after it had run for some time. The time discrepancy in detecting cells between the model runs and laboratory observations could be explained by the fact that LES only resolves eddies above grid scale. The disturbances imposed on the numerical model at release grew more slowly than the shorter wavelength disturbances possible in the laboratory environment, but grew more rapidly at later times when length scales had grown sufficiently large.

These structures are the consequence of an inherent *hydrostatic* instability caused by heavy fluid overlying light fluid in which all wavenumbers are unsTable. At the initial instant when motion has not yet started, this instability appears at all wavenumbers from that corresponding to the size of the thermal and will respond particularly to disturbance wavenumbers present. Each wavenumber present down to the fundamental mode defined by the source can draw on the available potential energy, so that we cannot be sure what motion will ensue, and in a small proportion of cases that motion may be far removed from any average. There is a strong tendency for structure to be conserved, expanding in size with time, and thus it should be regarded as unlikely that thermals would exhibit similarity over realizations, although they should certainly exhibit self-similarity. This suggests that we may be able to reduce the range of behaviour by increased care experimentally, but we should regard it as a significant feature of thermals released from rest. Non-buoyant puffs lack this source of potential energy and even buoyant vortex rings are to a significant degree stabilized by their source momentum. Strickly speaking, Richards' conclusion on the similarity between thermals and puffs is only valid for two-dimensional thermals which in reality do not exist.

Simulation of line puffs

We performed six tests on line puffs with initial momentum varied from $12.5 \rightarrow 28.0\ gcms^{-2}$. Although puffs are decelerating from the instant of release, they still required time to adjust to self-similar motion. As with line thermals, the line puffs travelled a distance of roughly one and a half times the source diameter before reaching their self-similarity regime. Figure 6 shows that puffs become self-similar at height $z = 0.83m$ with corresponding width $2r = 0.34m$. On average, once in their self-similarity stage, they maintained the rate of spreading until $2r = 0.60m$ and $z = 1.30m$ at which point the top wall begins to influence their growth. However, the stronger puffs which have more momentum spread less after $z = 1.10m$ and they also shows some influence of the top wall on their growth rate at $z = 1.30m$. The results from six tests gave values of the constant in the range $3.6 < n < 4.6$.

REFERENCES

Deardorff J.W.
Stratocumulus-capped mixed layers derived from a three-dimensional model.
Boundary-Layer Met., 18:495, 1980.

Gresho P.M.
Incompressible fluid dynamics: Some fundamental formulation issues.
Annu. Rev. Fluid Mec., 23:413, 1991.

Gresho P.M. and Sani R.L.
On pressure boundary conditions for the incompressible navier-stokes equations.
Int. J. for Numerical Methods in Fluids, 7:1111, 1987.

Harlow F.H. and Welch J.E.
Numerical calculation of time-dependent viscous incompressible flow of fluid with free surface.
Phys. Fluids, 8:2182, 1965.

Launder B.E. and Spalding D.B.
The numerical computation of turbulent flows.
Comp. Meth. in App. Mec. and Eng., 3:269, 1974.

Ng K.H. and Spalding D.B.
Turbulence model for boundary layers near walls.
The Physics of Fluids, 15:20, 1972.

Piacsek S.A. and Williams G.P.
Conservation properties of convection difference schemes.
J. Comp. Phys., 6:392, 1970.

Richards J.M.
Experiments on the motions of isolated cylindrical thermals through unstratified surroundings.
Int. J. Air Wat. Poll., 7:17, 1963.

Richards J.M.
Puff motions in unstratified surroundings
J. Fluid Mech., 21:97, 1965.

Tsang G.
Laboratory study of line thermals.
Atmos. Env., 5:445, 1971.

Wyngaard J.C. and Brost R.A.
Top-down and bottom-up diffusion of a scalar in the convective boundary layer.
J. Atmos. Sci., 41:102, 1984.

Zalesak S.T.
Fully multidimensional flux-corrected transport algorithms for fluids.
J. Comput. Phys., 31:335, 1979.

ACKNOWLEDGEMENTS

The authors would like to thank the National Greenhouse Advisory Committee for their financial support for the above work.

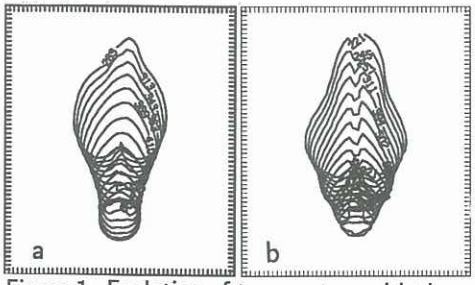

Figure 1. Evolution of temperature with time: (a) gaussian, (b) top hat thermals.

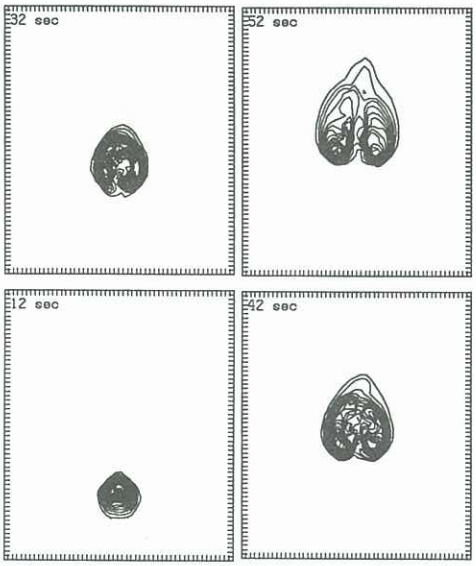

Figure 2. Cross-sectional plot of a gaussian thermal showing temperature contours at 12, 32, 42 and 52s after release.

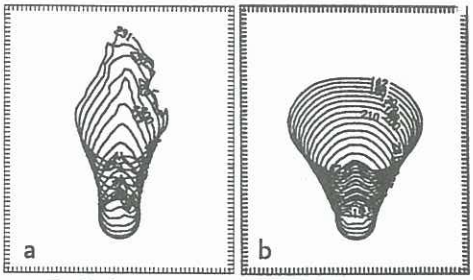

Figure 4. Evolution of temperature with time at different turbulent mixing coefficients: (a) low, (b) high.

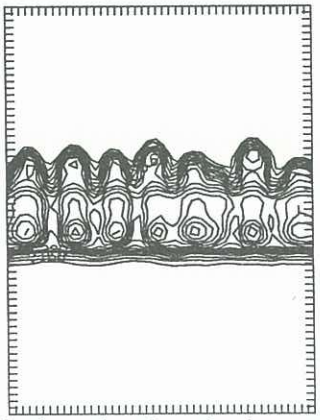

Figure 5. Isothermal surface plot demonstrating thermal instability along the axis.

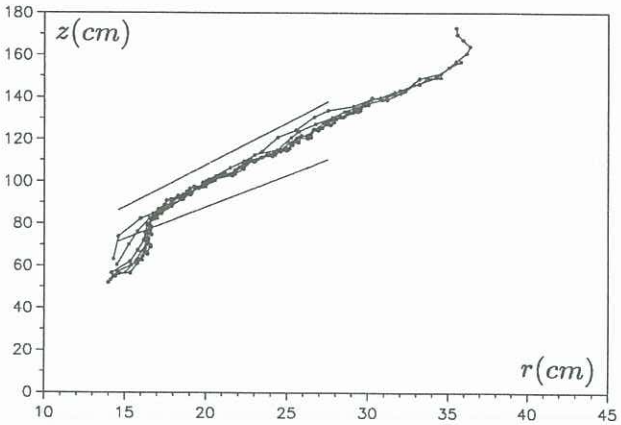

Figure 6. As in figure 3(a). But for puff motion.

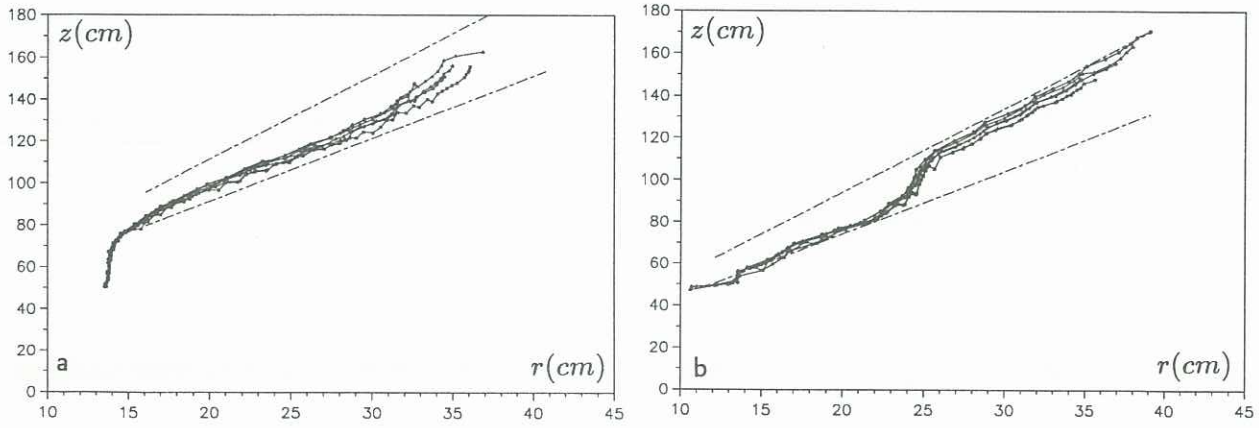

Figure 3. Relationship between the leading edge displacement (z) and halfwidth (r) for (a) gaussian, (b) top hat thermals. The slope of the data in the linear region gives the value of the constant n.